Fuel Processing Technology 205 (2020) 106452

Contents lists available at ScienceDirect

Fuel Processing Technology

journal homepage: www.elsevier.com/locate/fuproc

Research article

Investigation of the regeneration of a CO_2-loaded ammonia solution with solid acid catalysts: A promising alternative for reducing regeneration energy

Yin Xu[a,b,*], Baosheng Jin[a,**], Hejia Jiang[b], Lixiang Li[b], Juntao Wei[c]

[a] Key Laboratory of Energy Thermal Conversion and Control of Ministry of Education, School of Energy and Environment, Southeast University, Nanjing 210096, Jiangsu, China
[b] School of Electrical, Energy and Power Engineering, Yangzhou University, Yangzhou 225127, Jiangsu, China
[c] Institute of Clean Coal Technology, East China University of Science and Technology, Shanghai 200237, China

A B S T R A C T

Ammonia-based CO_2 capture is a promising option for suppressing CO_2 emissions from thermal power plants. However, the regeneration of a CO_2-loaded ammonia solution requires a large heat duty, hindering its industrial application. Herein, we investigated the regeneration of a CO_2-loaded ammonia solution with the aid of solid acid catalysts, i.e., protonated Zeolite Socony Mobil-5 (HZSM-5), γ-Al_2O_3, and TiO_2. The results demonstrate that all the catalysts can effectively promote the regeneration and the catalytic performance follows the trend: HZSM-5 > TiO_2 > γ-Al_2O_3. Especially, the presence of HZSM-5 can reduce the energy consumption by 23.9% compared to the non-catalytic regeneration. The catalysts were also characterized to reveal their various acid and textural properties. The characterization shows HZSM-5 possesses the most Brønsted acid sites amounting to 3143.8 μmol/g; while γ-Al_2O_3 has the most Lewis acid sites amounting to 3554.1 μmol/g. Furthermore, the relationships between the catalytic performance and catalyst properties were analyzed. Unlike amine-based regeneration, the CO_2 desorption rate increases linearly with the BET surface area × Brønsted acid sites. This is attributed to two factors: (1) smaller molecular volume of NH_2COO^-, and (2) a large proportion of HCO_3^- in the CO_2-loaded solution. Finally, a plausible catalytic mechanism was proposed. It suggested that Brønsted acid sites can provide accessible free protons to promote CO_2 released from HCO_3^- and CO_3^{2-}. However, the Brønsted acid sites and Lewis acid sites played a synergistic effect on the breakdown of NH_2COO^-.

1. Introduction

Capturing CO_2 discharged by coal-fired power plants has gained considerable attention for decades [1–4]. As a solution, three major technical routes have been developed, i.e., pre-combustion CO_2 capture, post-combustion CO_2 capture, and oxyfuel combustion [5,6]. Among these techniques, post-combustion CO_2 capture using amine solvents has been demonstrated on a commercial scale and considered as one of the most practical options [7–9]. However, this amine-based method still suffers several limitations such as high energy penalty and easy degradation [10]. To further improve the economic and technical feasibility, various alternative chemical solvents have been studied. The aqueous ammonia solution is considered as one of the most suitable options [11]. Compared with the conventional amine solvents, an aqueous ammonia solution has several advantages: low cost, low corrosiveness, resistance to degradation, high CO_2 loading capacity, and the potential of simultaneously removing multiple acid pollutants [12–14]. However, the NH_3-based CO_2 capture also faces two major challenges that hinder its large-scale application. One is the high volatility of NH_3, resulting in NH_3 escape, especially during the regeneration process with high operating temperature. The other challenge is that the regeneration duty of the ammonia-based process is theoretically evaluated to be < 2.5 MJ/kg CO_2 [15], however, the practical energy consumed is still too high to afford the task of capturing CO_2 on a large scale economically.

The regeneration duty of NH_3-based process involves three parts: (1) the desorption heat to break chemical bonds in CO_2-absorbed products, (2) the sensible heat to raise the temperature of the CO_2-loaded solution, and (3) the vaporization heat to produce the water vapor [16,17]. Evidently, except for the desorption heat, suppressing the sensible heat and the vaporization heat is crucial for reducing regeneration duty. Numerous efforts have been devoted to reducing regeneration duty. Jilvero et al. [15] found that pressurized regeneration can lower the heat requirement due to the suppression of water evaporation. Zhang and Guo [18] and Yu and Wang [19] numerically investigated the optimal operating parameters for the minimum regeneration duty, respectively. To improve the energy performance, Li et al. [16] integrated the rich-split process and the inter-heating process

* Correspondence to: Y. Xu, School of Electrical, Energy and Power Engineering, Yangzhou University, Yangzhou 225127, Jiangsu, China.
** Corresponding author.
E-mail addresses: 006307@yzu.edu.cn (Y. Xu), bsjin@seu.edu.cn (B. Jin).

https://doi.org/10.1016/j.fuproc.2020.106452
Received 30 December 2019; Received in revised form 26 March 2020; Accepted 12 April 2020

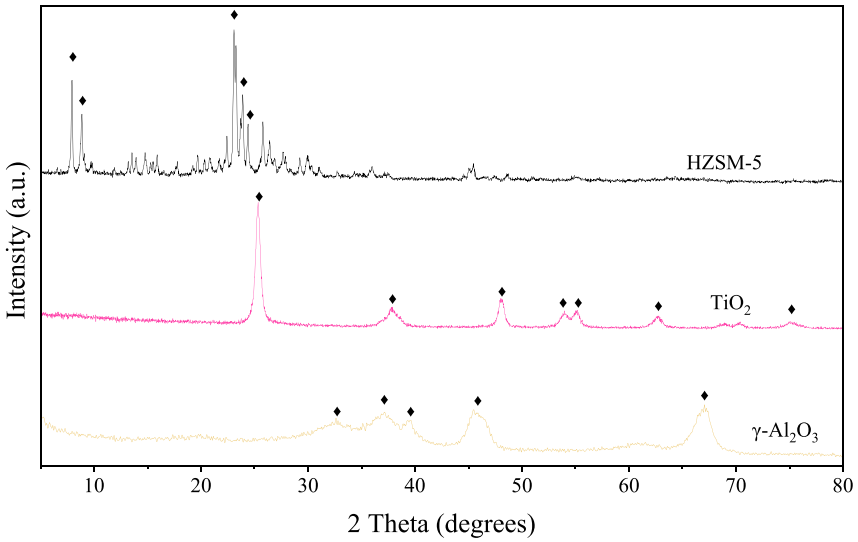

Fig. 1. XRD patterns of HZSM-5, TiO_2, and γ-Al_2O_3.

into the regeneration process, and later they proposed an advanced flash stripping process [20]. Moreover, Zhang and Guo [21] introduced a flow-by capacitive ion separation device into the regeneration process.

Although the proposed strategies can substantially reduce the regeneration duty, there is still a significant gap from the desired level. More recently, solid acid catalysts have been introduced into the regeneration of amine solvents. Conventionally, the regeneration of the amine solvent runs at a temperature of 120–140 °C. Since the solid acid catalysts can promote the breakdown of CO_2 absorbed products, the regeneration temperature can be operated below 100 °C, which leads to lower sensible heat and less water evaporation [22]. Shi et al. [23] investigated the effects of γ-Al_2O_3 and protonated Zeolite Socony Mobil-5 (HZSM-5) on the regeneration of the amine solvent. They found that the presence of the solid acid catalysts reduces the regeneration duty by 62% compared to non-catalytic regeneration. Liang et al. [24] experimentally studied the regeneration of CO_2-loaded MEA solution with single and hybrid acid solid catalysts. They suggested that the catalytic performance should be affected by joint characteristics of solid acid catalysts. Liu et al. [25] compared the performance of three solid acid catalysts, i.e., HZSM-5, Mobil Composition of Matter No. 41 (MCM-41), and SO_4^{2-}/ZrO_2, in the regeneration of single and blended amine solvents. They found that even though HZSM-5 had moderate acid sites, it showed the best performance. They further attributed this to the high ratio of the Brønsted acid sites to the Lewis acid sites (B/L) and mesopore surface area of HZSM-5. Bhatti et al. [26] studied five transition metal oxides as solid acid catalysts for the regeneration of a CO_2-loaded MEA solution. The experimental results implied that these transition metal oxides should play a vital role in reducing the regeneration duty by providing Brønsted/Lewis acid sites. Lai et al. [27] investigated the influence of the nanostructure $TiO(OH)_2$ on the regeneration of the CO_2-loaded MEA solution. They reported that $TiO(OH)_2$ could remarkably reduce the regeneration duty. Prasongthum et al. [28] compared a solid superacid catalyst $Ce(SO_4)_2/ZrO_2$ with HZSM-5 in the regeneration of Bi-blended amine solvents. They found $Ce(SO_4)_2/ZrO_2$ exhibited much better performance due to more Brønsted acid sites and larger pore size.

Although increasing attention has been paid to the regeneration process with the aid of solid acid catalysts, most studies focus on the conventional amine solvent. The influences of solid acid catalysts on the regeneration of CO_2-loaded ammonia solutions are still scarcely reported. Particularly, lowering the regeneration temperature can further suppress NH_3 escape. Therefore, the aim of this work is to reveal the effects of solid acid catalysts on the regeneration of CO_2-loaded ammonia solution. Three solid acid catalysts, i.e., HZSM-5, TiO_2, and γ-Al_2O_3, were investigated experimentally. Furthermore, the relationships between the catalytic performance and the properties of the catalysts were analyzed, and a catalytic mechanism was also proposed to explain the catalytic performance.

2. Materials and methods

2.1. Chemicals

Ammonium hydroxide solution with analytical grade was purchased from Sinopharm Chemical Reagent Co., Ltd. γ-Al_2O_3 (purity ≥ 95%) was acquired from Shanghai Macklin Chemical Reagent Co. Ltd., China. TiO_2 (purity > 98%) was obtained from Shanghai Dingfen Chemical Technology Co., Ltd. HZSM-5 with Si/Al molar ratio of 20 was purchased from Tianjin Nankai University Catalyst Co. Ltd., China. This commercial HZSM-5 was conventionally modified from ZSM-5 precursor zeolite ($Na_nAl_nSi_{96-n}O_{192}{\cdot}H_2O$, $0 < n < 27$) [29]. Through ion-exchange and calcination, the Na^+ cations in the precursor zeolite can be replaced by H^+ forming HZSM-5 [30]. N_2 and CO_2 with a purity of 99% were purchased from Nanjing Special Gas Co., Ltd. Before experiments, all the solid acid catalysts were dried at 105 °C for 4 h, and then calcined for another 2 h at 400 °C. Later, these solid acid catalysts were characterized by X-ray diffraction (XRD) as shown in Fig. 1. As can be seen, HZSM-5 has the diffraction peaks at 2 theta of 7.9°, 8.8°, 23.1°, 23.7°, and 24.4°; TiO_2 possesses the diffraction peaks at 2 theta of 25°, 38°, 48°, 53°, 55°, 63°, and 75°; γ-Al_2O_3 presents the diffraction peaks at 2 theta of 32.5°, 37.3°, 39.3°, 45.7°, 66.8°. These diffraction peaks of these solid acid catalysts are in an excellent agreement with the standard patterns and literature data, respectively [31–34].

2.2. Preparation of CO_2-loaded solution

A fresh 2.86 mol/L (5 wt%) ammonia solution with the volume of 1 L was firstly prepared through the weighting method. Then, a stream of CO_2 at 0.5 L/min was introduced into the solution for about 1 h at room temperature to prepare a CO_2-loaded solution with CO_2 loading of 0.5 mol CO_2/mol NH_3. To ensure the desired CO_2 loading, when the absorption time is over 50 min, 2 mL solution was pipetted every 2 min and titrated by 1 mol/L HCl solution to determine the CO_2 loading of the solution. Typically, the actual CO_2 loading is in the range of 0.495–0.505 mol CO_2/mol NH_3. The prepared CO_2-loaded solution was

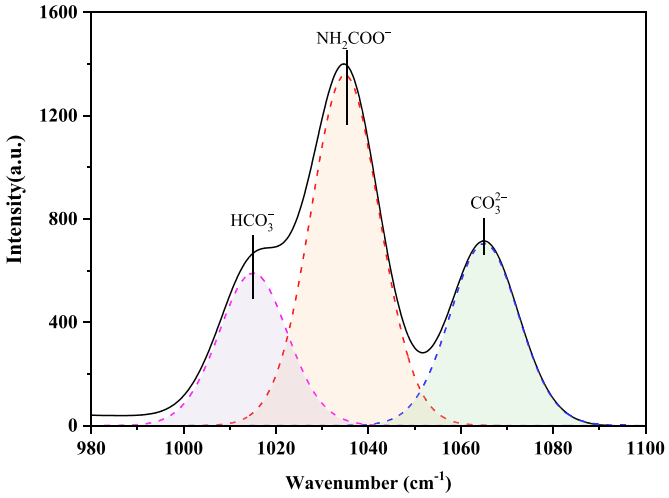

Fig. 2. Raman spectra of prepared CO_2-loaded solution with the CO_2 loading of 0.5 mol CO_2/mol NH_3.

Table 1
Experimental and calculated concentrations of species in the prepared CO_2-loaded solution. The experimental values were determined by the integrated band area; the calculated values were evaluated from the thermodynamic model of NH_3-CO_2-H_2O system.

$C(HCO_3^-)$ mol/L		$C(NH_2COO^-)$ mol/L		$C(CO_3^{2-})$ mol/L	
Exp.	Cal.	Exp.	Cal.	Exp.	Cal.
0.501	0.542	0.655	0.710	0.273	0.178

further analyzed by Raman spectroscopy as shown in Fig. 2. The bands at 1017 cm^{-1}, 1034 cm^{-1}, and 1065 cm^{-1} are ascribed to HCO_3^-, NH_2COO^-, and CO_3^{2-}, respectively [35]. The concentrations of these species can be determined by the integrated band area using the method proposed by Wen and Brooker [35], and their values are summarized in Table 1. These concentrations can also be theoretically evaluated from the thermodynamic model of the NH_3-CO_2-H_2O system [36], which are also presented in Table 1. There are slight differences between the calculated and experimental concentrations. However, the trend in the species distribution is similar. That is, NH_2COO^- is the major product, followed by HCO_3^- and CO_3^{2-}.

2.3. Experimental apparatus and procedure

The schematic diagram of the regeneration system was shown in Fig. 3. A stream of N_2 was introduced into the regeneration system as a carrier gas, and its flow rate was maintained at 2 L/min by a mass flowmeter. The regeneration reactor was immersed in the oil bath. The regeneration temperature was set at 70 °C and regulated by a PID controller. Besides, a magnetic agitator with a constant stirring speed of 500 rpm was used to make species and temperature uniform during the regeneration process. In order to minimize the heating period, the reactor was preheated to 75 °C, and then 150 mL CO_2-loaded solution mixed with 7.5 g solid acid catalysts were poured into the regeneration reactor. During the experiments, the CO_2 concentration in the outlet gas was measured by an infrared gas analyzer (SIEMENS, Ultramat 6E) and the molar rate of CO_2 desorbed was calculated by Eq. (1).

$$N_{CO_2} = N_{N_2} \frac{y_{CO_2}}{(1 - y_{CO_2})} \quad (1)$$

where N_{N2} is the molar rate of N_2 calculated by the volume flow rate, and y_{CO2} is the volume fraction of CO_2. The variation of solution temperature was detected by a K type thermocouple and the energy consumption was measured by an electric energy meter with the accuracy 0.001 kWh.

2.4. Catalyst characterization

All the catalysts were characterized in terms of X-ray diffractometer (XRD) patterns, BET specific area, pore volume and diameter, and Pyridine-adsorbed Fourier Transform Infrared Spectra (Py-FTIR). XRD patterns of the catalysts were recorded on a D8 ADVANCE X-ray diffractometer (Bruker, Germany) using Cu *K*α radiation (40 kV, 40 mA) in the 2θ range from 5° to 80°. A continuous mode was used with a scan speed of 8°/min and 2θ angle of 0.02° at 25 °C. BET specific area, pore volume and pore diameter were determined by the nitrogen adsorption/desorption method at −196 °C using an Autosorb IQ3 (Quantachrome Instruments, America). Prior to the measurement, the samples were degassed at 200 °C for 2 h. The Pyridine-adsorbed Fourier Transform Infrared Spectra were obtained from a Nicolet 380 (Thermo Scientific, America). Before the test, each sample was treated in a vacuum at 450 °C for 5 h to remove physically adsorbed species. After the pretreatment, the sample was cooled to room temperature and then absorbed pyridine for 60 min. When the absorption was completed, desorption was carried out for 2 h in a vacuum at 150 °C to remove physically adsorbed pyridine. After that, the IR spectra of the sample were measured in the Nicolet 380 with the wavenumber 600–4000 cm^{-1}, 4 cm^{-1} resolutions, and 32 scans. The amount of Brønsted acid sites and Lewis acid sites were calculated from the areas of IR bands at ca. 1450 cm^{-1} and 1540 cm^{-1}, respectively. Subsequently, the desorbed temperatures were further elevated to 250 °C and 350 °C, and the corresponding concentrations of Brønsted acid sites and Lewis acid sites at these conditions were also evaluated using the same methods.

3. Results and discussion

3.1. CO_2 desorption performance

Fig. 4 shows the regeneration of CO_2-loaded ammonia solutions with and without the catalysts at the temperature of 70 °C, and the initial CO_2 loading of the solution is 0.5 mol CO_2/mol NH_3. Since the desorbed CO_2 is continuously removed by carrier gas N_2, all the curves of CO_2 loading decrease with time and approach to completed desorption. Generally, all the regeneration cases with the presence of solid acid catalysts exhibit better performance than the blank case. HZSM-5 exhibits the best catalytic performance followed by TiO_2 and γ-Al_2O_3. However, during the temperature ramp-up stage, the catalytic performance is less impressive and their curves are close to the curve of the blank case. This indicates that the desorbing temperature is of importance at this stage. When the temperature rises to about 70 °C, the catalytic effects become prominent. This trend is also observed in the catalytic regeneration of MEA solution. It is reported that the catalysts exhibit better performance when the desorbing temperature is over 65 °C [26]. At the end of the isothermal stage, the CO_2 desorption rate slows down due to the reduction of the driving force for CO_2 regeneration.

The amount of CO_2 desorbed, regeneration duty, and average CO_2 desorbing rate during the regeneration are summarized in Table 2. Fig. 5 shows the comparisons of the relative heat required from the regeneration with and without the catalysts. The regeneration in the absence of catalysts is used as the baseline. As can be seen, the results prove that the solid acids can reduce the regeneration energy consumed and accelerate CO_2 desorption. The reduced relative heat required is in the order of: blank case (100%) > γ-Al_2O_3(91.9%) > TiO_2(79.6%) > HZSM-5(76.1%). Besides, according to Table 2, the average CO_2 desorbing rate at the presence of HZSM-5 is also the fastest, amounting to 2.34 mmol/min.

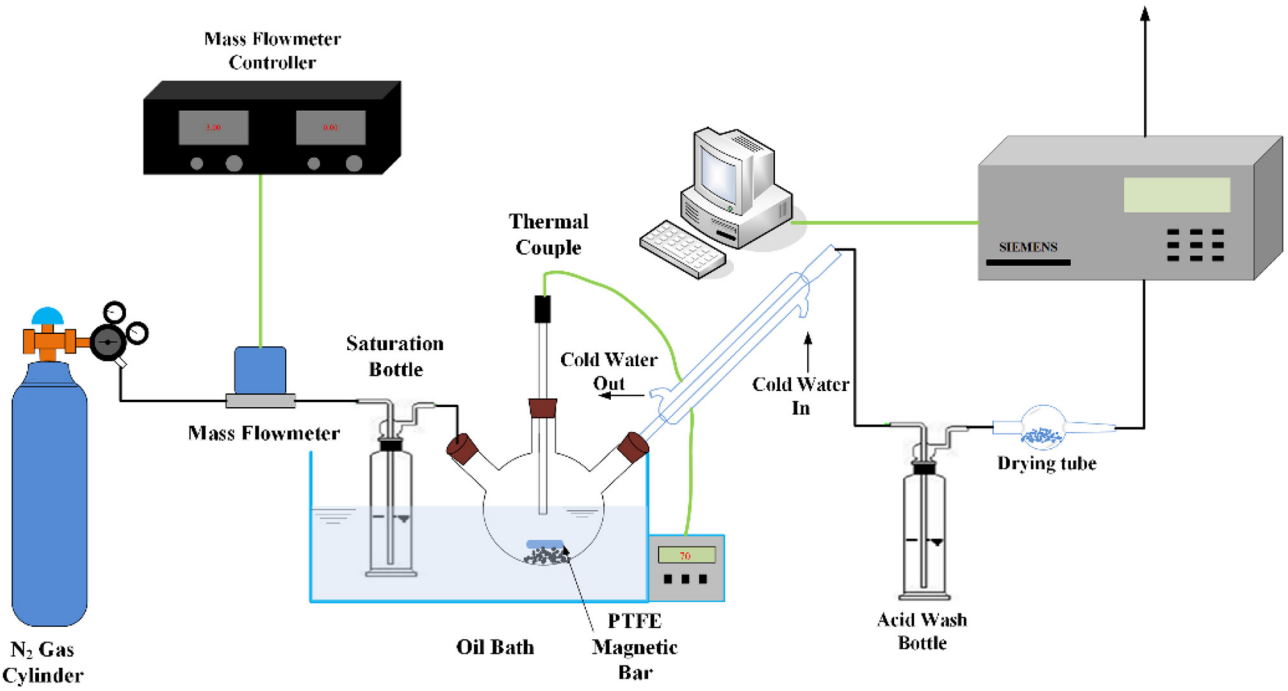

Fig. 3. Schematic diagram of the regeneration system.

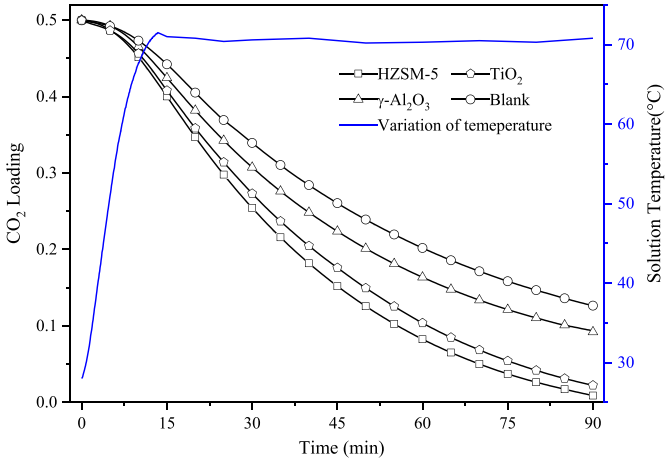

Fig. 4. Regeneration of CO_2-loaded ammonia solutions with and without the catalysts at the temperature of 70 °C and the initial CO_2 loading of 0.5 mol CO_2/mol NH_3.

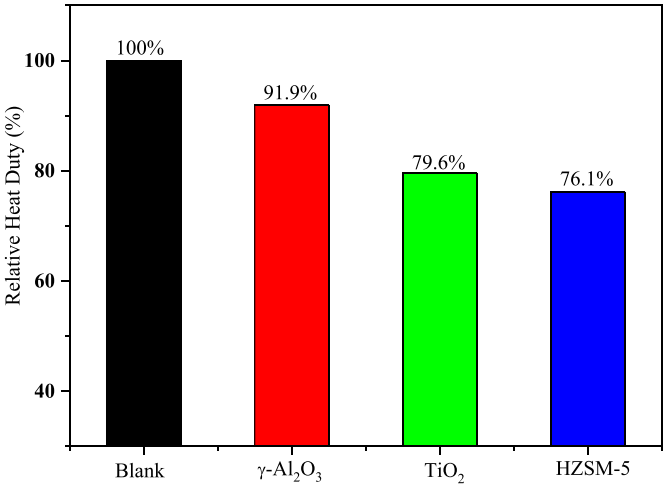

Fig. 5. Comparisons of Relative heat duty for the regeneration of CO_2-loaded ammonia solutions with and without acid solid catalysts at the temperature of 70 °C and initial CO_2 loading of 0.5 mol CO_2/mol NH_3.

Table 2
Summary for the amount of CO_2 desorbed, Heat duty, and average CO_2 desorbing rate during the 90 min regeneration at a temperature of 70 °C and CO_2 loading of 0.5 mol CO_2/mol NH_3.

Catalyst	Amount of CO_2 desorbed (mol)	Regeneration duty (kJ/mol CO_2)	Average CO_2 desorption rate (mmol/min)
Blank case	0.160	2527.2	1.78
HZSM-5	0.211	1922.4	2.34
TiO_2	0.201	2012.0	2.23
γ-Al_2O_3	0.174	2322.4	1.93

3.2. Catalytic properties of solid acid catalysts

The acidic properties of the solid acid catalysts were probed by the pyridine adsorption technique. Pyridine can be adsorbed on the surface of these catalysts via two different pathways [37]. One is that pyridine can coordinate with the unsaturated metal sites, the Lewis acid sites, which shows the band around 1450 cm^{-1}. The other is that pyridine can react with the acidic OH groups, the Brønsted acid sites, to form pyridinium ion, which shows the band around 1540 cm^{-1}. Additionally, the bands around 1490 cm^{-1} are ascribed to the joint effect of Lewis and Brønsted acid sites [25,38]. Fig. 6 shows the FT-IR spectra of pyridine-adsorbed HZSM-5, γ-Al_2O_3, and TiO_2. In Fig. 6, there are both appreciable bands around 1450 cm^{-1} and 1540 cm^{-1} in the spectra of pyridine-adsorbed HZSM-5 and TiO_2, indicating HZSM-5 and TiO_2 have both Lewis and Brønsted acid sites. However, it is noted that the origin of the Brønsted acid sites on the surface of HZSM-5 and TiO_2 is different. The Brønsted acid sites on HZSM-5 originate from the acidic OH groups located between Al and Si on the zeolite structure [28]; whereas the Brønsted acid sites on TiO_2 result from the reaction with water molecule, converting the surface oxides into OH groups [39].

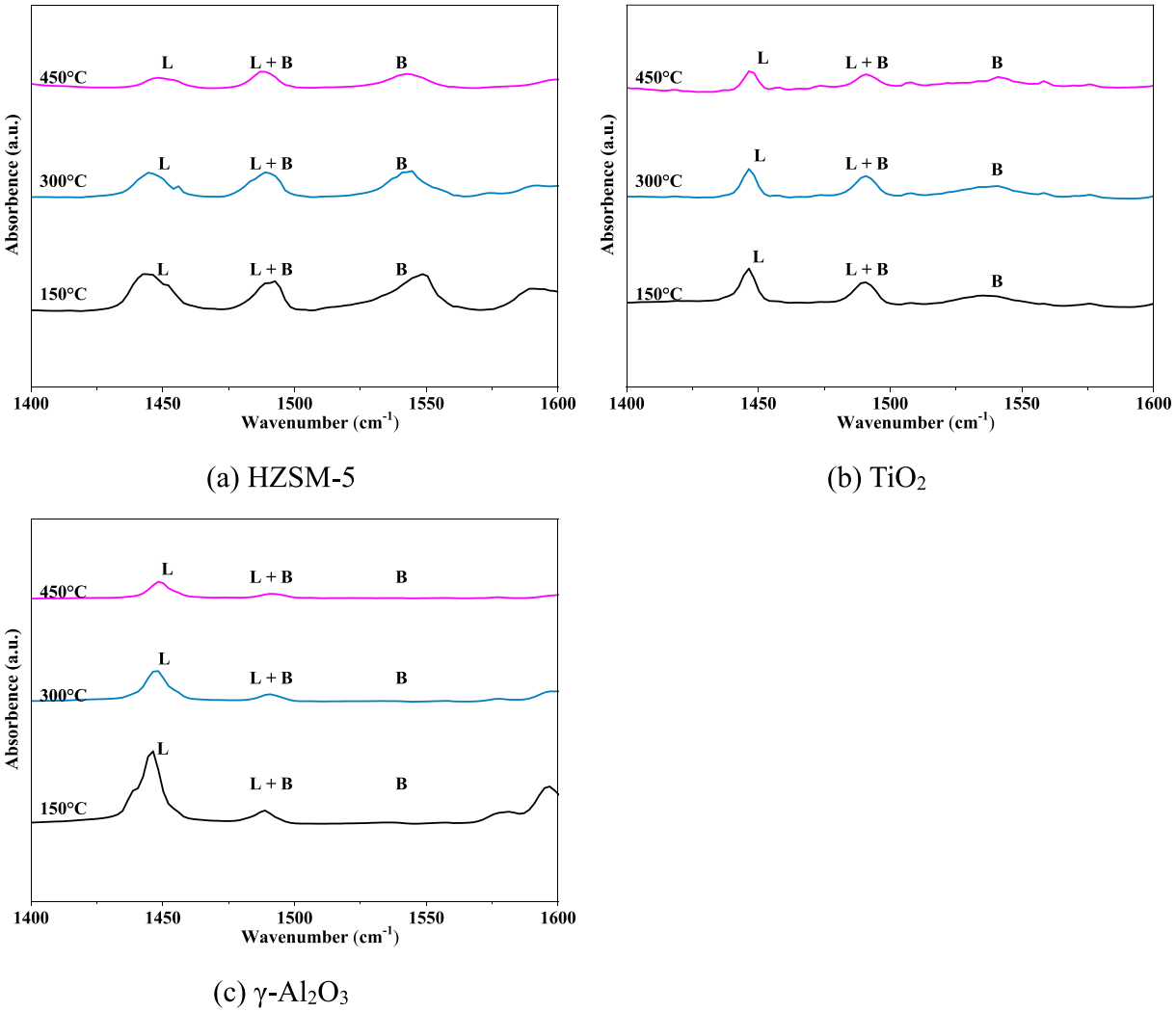

Fig. 6. FT-IR spectra of pyridine-adsorbed (a)HZSM-5, (b)TiO_2, and (c)γ-Al_2O_3.

Table 3
Acidic properties of HZSM-5, TiO_2, and γ-Al_2O_3.

Catalyst	Brønsted acid sites μmol/g			Lewis acid sites μmol/g			Total acid sites μmol/g		
	Weak	Medium	Strong	Weak	Medium	Strong	B	L	B/L
HZSM-5	1397.3	629.0	1117.5	662.0	601.2	495.1	3143.8	1758.3	1.79
TiO_2	404.8	319.7	562.8	354.6	508.3	525.8	1287.3	1388.7	0.93
γ-Al_2O_3	42.0	31.5	35.7	1991.3	737.8	825.0	109.2	3554.1	0.031

Besides, there are only obvious bands at 1450 cm^{-1} in the spectra of pyridine-adsorbed γ-Al_2O_3. This suggests that γ-Al_2O_3 mainly possess the Lewis acid site. Furthermore, the amount of Lewis and Brønsted acid sites can be determined by the area of the bands at 1450 cm^{-1} and 1540 cm^{-1}, respectively, using the Lambert–Beer law [28] (details provided in Supplementary material). The calculated results are summarized in Table 3. As can be seen in Table 3, HZSM-5 has the highest amount of Brønsted acid sites while the γ-Al_2O_3 possesses the highest amount of Lewis acid sites. Besides, the B/L ratio of HZSM-5 amounts to 1.79, suggesting Brønsted acid sites are dominant on HZSM-5. In contrast, the B/L ratio of γ-Al_2O_3 is close to 0, indicating that there are almost no Brønsted acid sites on γ-Al_2O_3. We also desorbed pyridine at different temperatures, i.e., 150 °C, 300 °C, and 450 °C, to probe the amount of weak, medium, and strong acid sites. As shown in Table 3, the distribution of the strength of the three solid acids is quite different. The Lewis acid sites on γ-Al_2O_3 are mainly weak acid sites and the weak Brønsted acid sites are also dominant on HZSM-5. In comparison with HZSM-5 and γ-Al_2O_3, the acid strength on TiO_2 is more evenly distributed.

The textural properties of the catalysts were measured by N_2 adsorption/desorption method. Fig. 7 shows the N_2 adsorption-desorption isotherms for the catalysts. According to the IUPAC report [40], the N_2 adsorption-desorption isotherms of the three catalysts belong to the type IV isotherms, indicating the three catalysts possess mesoporous structures. Besides, the narrow hysteresis loop presented in the isotherms of HZSM-5 and TiO_2 implies the enrichment of micropores in these catalysts, while the large hysteresis loop in the isotherms of γ-Al_2O_3 suggests the domination of mesopores. Table 4 further summaries the calculated textural properties of the three catalysts. As can be seen, the textural properties of the three catalysts are quite different. TiO_2 has

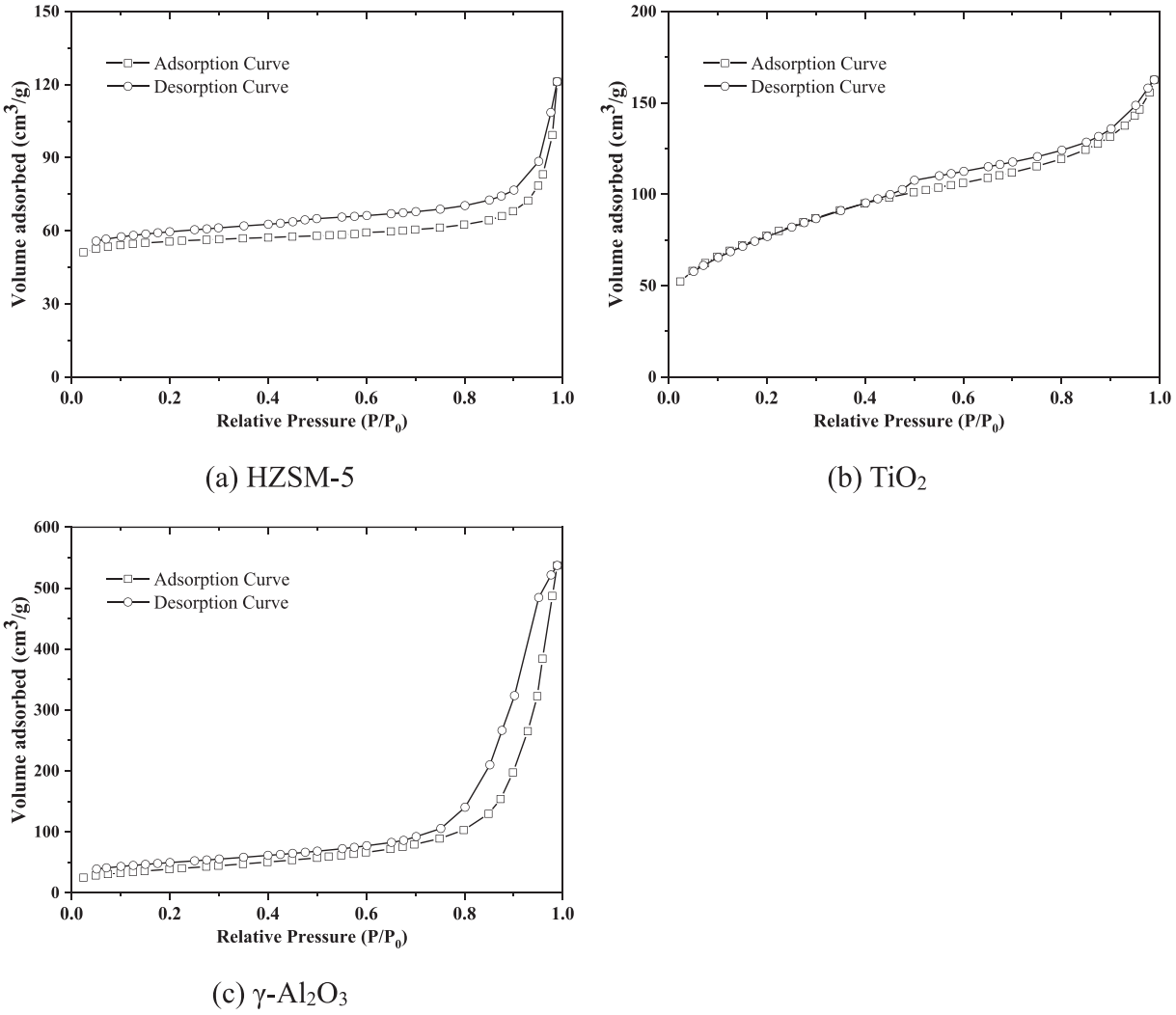

Fig. 7. N_2 adsorption-desorption isotherms: (a) HZSM-5, (b) TiO_2, and (c) γ-Al_2O_3.

Table 4
The textural properties of the three solid catalysts.

Catalyst	Surface area m^2/g			Pore volume cm^3/g	Average pore diameter (nm)
	S_{micro}	S_{meso}	S_{BET}		
HZSM-5	153.2	16.4	169.6	0.19	4.42
TiO_2	102.3	169.3	271.6	0.25	3.70
γ-Al_2O_3	1.3	137.9	139.2	0.83	23.88

the largest BET surface with a comparable microporous and mesoporous surface. HZSM-5 mainly possesses a microporous surface, while a mesoporous surface is dominant on γ-Al_2O_3. However, TiO_2 has the smallest average pore diameter, only 3.70 nm. It is noted that extreme small pore diameter will prevent the products from accessing the activated sites.

3.3. Relationships between catalytic performance and catalysts properties

After characterizing and testing the catalysts, it is necessary to figure out which properties of the catalysts have a crucial influence on the catalytic performance. Thus, we correlated the properties of the catalysts with the average CO_2 desorption rate. For the influence of a single property, we found that the average desorption rate was weakly related to pore volume, pore diameter, BET surface area, and Lewis acid sites, respectively (as shown in Supplementary material), indicating these properties hardly affect the CO_2 desorption alone. It was also found that the average desorption rate nonlinearly increases with the increasing Brønsted acid sites as shown in Fig. 8. This trend was also

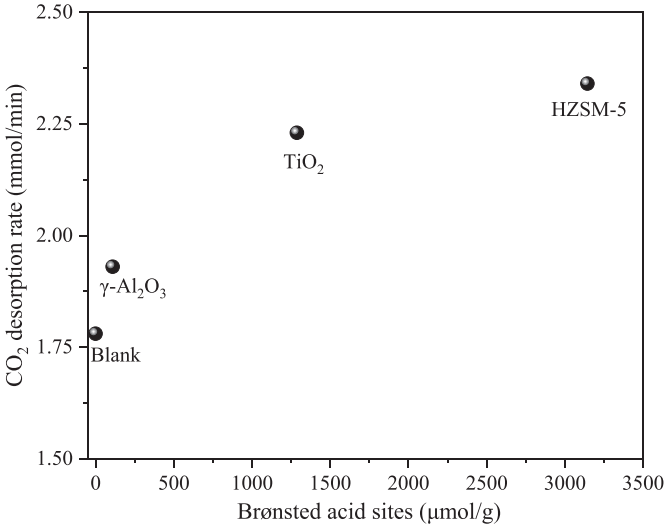

Fig. 8. The relationship between CO_2 desorption rate and Brønsted acid sites.

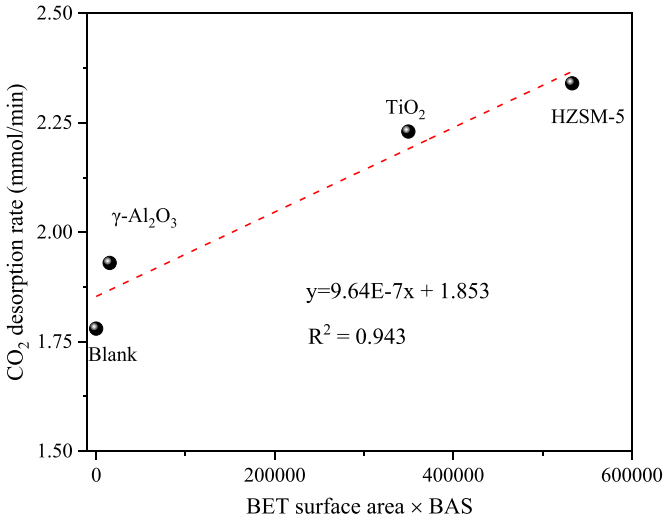

(a) BET surface area×BAS

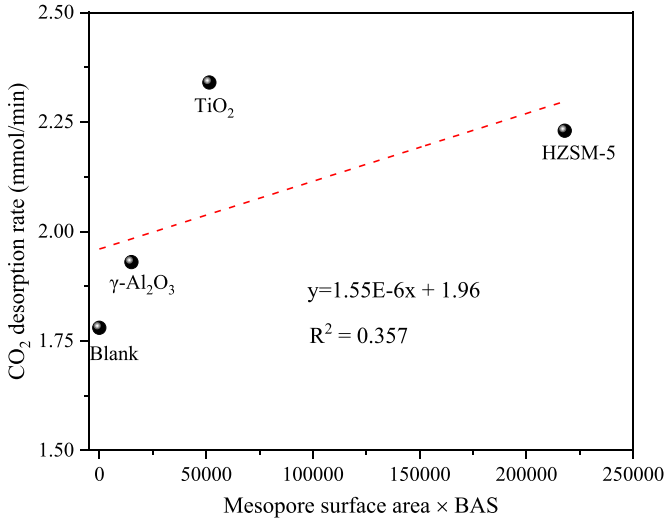

(b) mesopore surface area×BAS

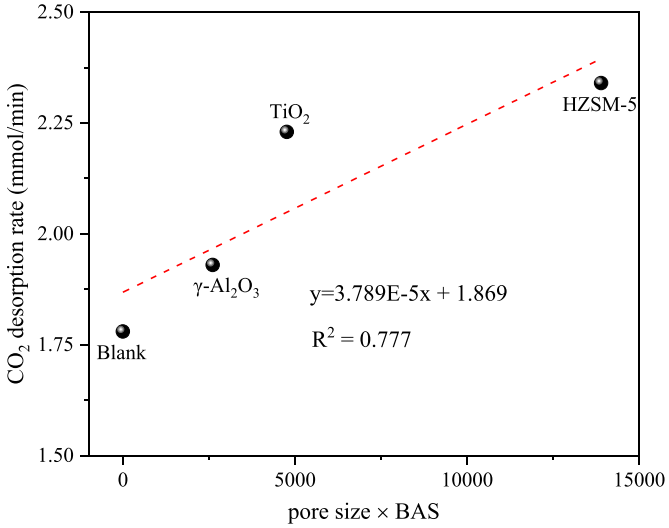

(c) pore size×BAS

Fig. 9. The relationships between CO_2 desorption rate and the jointed effects: (a) BET surface area × BAS, (b) mesopore surface area × BAS, and (c) pore size × BAS.

observed in the catalytic MEA-based CO_2 desorption process [17,41]. This is because the more Brønsted acid sites, the more protons are available for the CO_2 desorption. Particularly, considering a large portion of HCO_3^- exists in the NH_3-based CO_2-loaded solution, the Brønsted acid sites can effectively promote the CO_2 desorption. Natthawan et al. [28] reported that the average pore diameter also had a significant influence on the MEA-based CO_2 desorption. However, this phenomenon was not observed in this work. This is probably because NH_2COO^- has a small molecular volume as compared to $MEACOO^-$. Besides, the nonlinear relationship between the desorption rate and Brønsted acid sites implies that the desorption rate is not determined by Brønsted acid sites alone.

The combined effects of these catalyst properties were also considered to play an important role in previous studies [17,28]. The product of two catalyst properties was investigated, including BET surface area × Brønsted acid sites (BAS), mesopore surface area × BAS, and pore size × BAS. Fig. 9 shows the correlation between the desorption rate and the combined effects. Herein, we found that the average desorption rate is weakly related to the mesopore surface area × BAS, while it increases with the increasing BET surface area × BAS and pore size × BAS. Particularly, there is an apparent linear relationship between the desorption rate and BET surface area × BAS. This linear relationship suggests the combined effect of BET surface area and BAS play a crucial role in the ammonia-based CO_2 desorption. It is also noted that Liang et al. [42] found that the product of mesopore surface area and total acid sites plays the most critical role in amine-based CO_2 desorption. The differences between our findings and the conclusions of Liang et al. [42] can be attributed to two reasons. One is that the smaller molecular volume of NH_2COO^- decreases the lower limit of pore size, increasing the accessibility of micropore surface area. The other reason is that, there is a large portion of HCO_3^- in ammonia-based CO_2-loaded solution. With the proton supplied by Brønsted acid sites, HCO_3^- can easily decompose into CO_2 and H_2O. In contrast, $MEACOO^-$ is the dominant component of the MEA-based CO_2-loaded solution. According to the desorption mechanisms proposed by Liang et al. [42], both Brønsted acid sites and Lewis acid sites are essential in the breakdown of $MEACOO^-$.

3.4. Analysis of the catalytic mechanism

According to the literature, the NH_3-based CO_2 absorption occurs through a series of proton-transfer reactions, generating NH_4^+, HCO_3^-, NH_2COO^-, and CO_3^{2-} [43]. Thus, for the desorption, protons should be reversely liberated from NH_4^+ and transferred to HCO_3^-, NH_2COO^- and CO_3^{2-}. However, the direct deprotonation of NH_4^+ is difficult due to a high reaction barrier [17], leading to the lack of free protons. With the addition of acid catalysts, Brønsted acid sites can provide available protons. When obtaining free protons, HCO_3^- and CO_3^{2-} can be easily converted to H_2CO_3, which can further release CO_2. Besides, the Brønsted acid sites that lost protons can acquire protons from NH+ 4. In this whole process, Brønsted acid sites act as proton shuttles, which can effectively reduce the reaction barrier. Thus, for the CO_2 desorption from HCO_3^- and CO_3^{2-}, Brønsted acid sites play more important roles than Lewis acid sites. This can explain why Brønsted acid sites are preferred in the regeneration of a CO_2-loaded NH_3 solution.

For the breakdown of NH_2COO^-, the process is more complicated. Besides the free protons, the cleavage of the C—N bond is also required. A possible catalytic mechanism for the breakdown of NH_2COO^- is schematically described in Fig. 10. Firstly, NH_2COO^- is adsorbed on the Brønsted acid sites and then obtains the proton, forming NH_2COOH. Subsequently, the Lewis acid sites, the unsaturated mental atoms, rob the lone pairs of electrons of N atom and O atom. This results in the rehybridization of N atom from sp^2 to sp^3 [39], weakening the C—N bond and strengthening the C—O bond. Besides, the NH_2COOH will be isomerized, and the H atom bonded with the O atom will be shifted toward the N atom. Finally, the C—N bond is broken, and the NH_2COOH

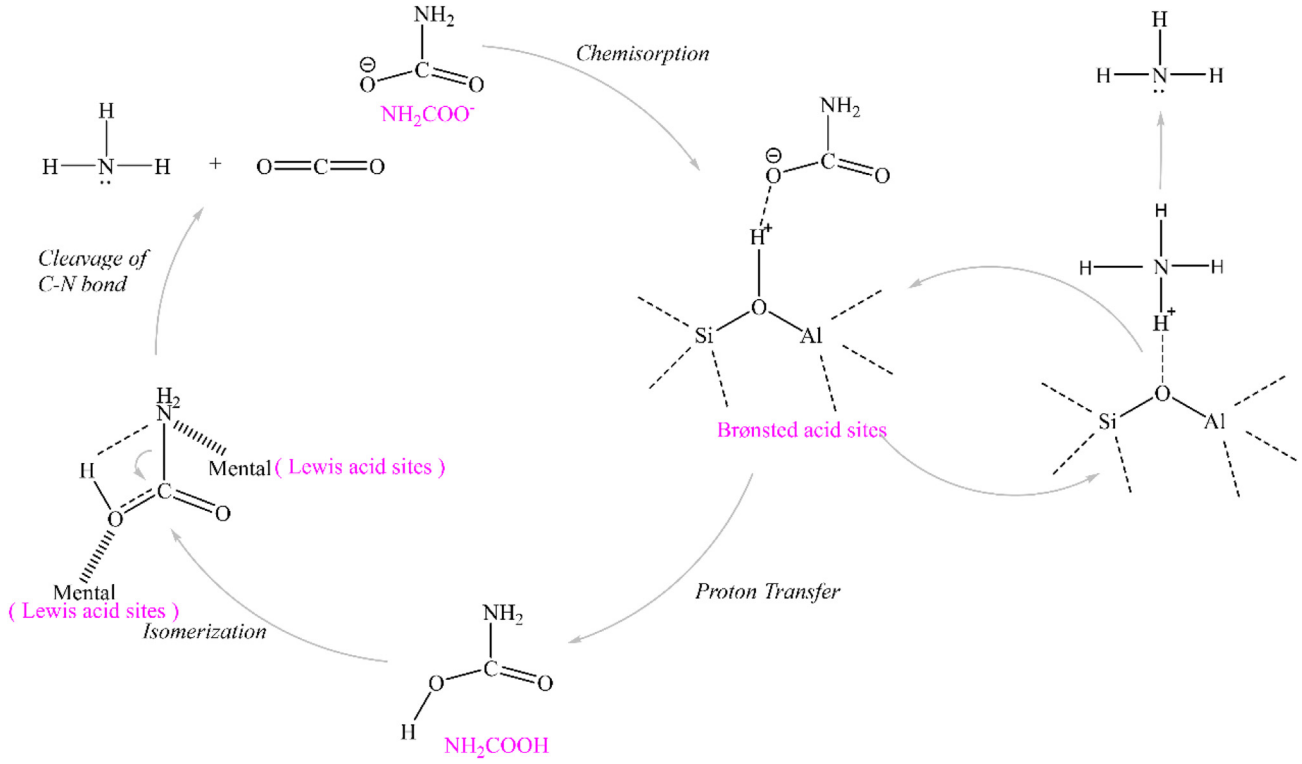

Fig. 10. A possible catalytic mechanism for the breakdown of NH_2COO^-.

is divided into NH_3 and CO_2. In this process, the Brønsted acid sites and Lewis acid sites synergistically assist the breakdown of NH_2COO^-.

4. Conclusions

In this work, we have investigated the regeneration of CO_2-loaded ammonia solutions with the aid of solid acid catalysts. It was found that these catalysts can effectively promote the regeneration process, reducing the energy consumed and accelerating CO_2 desorption. The catalytic performance was ranked as: HZSM-5 > TiO_2 > γ-Al_2O_3. The characterization showed that the acidic and textural properties of the catalysts were significantly different. Furthermore, the relationship between catalytic performance and catalysts properties was analyzed. For a single property, the CO_2 desorption rate nonlinearly increases with the increasing Brønsted acid sites. For the combined effect of the properties, unlike the regeneration of the MEA solution, the CO_2 desorption rate increases linearly with the BET surface area × Brønsted acid sites. This is due to two factors: (1) smaller molecular volume of NH_2COO^-, and (2) large proportion of HCO_3^- in the CO_2-loaded NH_3 solution. Finally, a possible catalytic mechanism was proposed. It suggested that Brønsted acid sites can provide accessible free protons to promote CO_2 released from HCO_3^- and CO_3^{2-}. However, the Brønsted acid sites and Lewis acid sites played a synergistic effect on the breakdown of NH_2COO^-.

CRediT authorship contribution statement

Yin Xu:Conceptualization, Methodology, Formal analysis, Writing - original draft.**Baosheng Jin**:Conceptualization.**Hejia Jiang**:Investigation.**Lixiang Li**:Investigation.**Juntao Wei**:Writing - review & editing.

Declaration of competing interest

The authors declare that they have no known competing financial interests or personal relationships that could have appeared to influence the work reported in this paper.

Acknowledgements

The authors are very grateful to the National Natural Science Foundation of China (Grant No. 51806188 and No. 51276038), the Natural Science Foundation of Jiangsu Province of China (Grant No. BK20180932), the Natural Science Foundation of the Jiangsu Higher Education Institutions of China (Grant No. 18KJB470025), and Jiangsu Provincial Government Scholarship Program for financial support.

Appendix A. Supplementary data

Supplementary data to this article can be found online at https://doi.org/10.1016/j.fuproc.2020.106452.

References

[1] W. Srisang, F. Pouryousefi, P.A. Osei, B. Decardi-Nelson, A. Akachuku, P. Tontiwachwuthikul, R. Idem, Evaluation of the heat duty of catalyst-aided amine-based post combustion CO_2 capture, Chem. Eng. Sci. 170 (2017) 48–57.
[2] F.A. Rahman, M.M.A. Aziz, R. Saidur, W.A.W.A. Bakar, M.R. Hainin, R. Putrajaya, N.A. Hassan, Pollution to solution: capture and sequestration of carbon dioxide (CO_2) and its utilization as a renewable energy source for a sustainable future, Renew. Sust. Energ. Rev. 71 (2017) 112–126.
[3] B. Zhao, Y. Su, W. Tao, L. Li, Y. Peng, Post-combustion CO_2 capture by aqueous ammonia: a state-of-the-art review, International Journal of Greenhouse Gas Control 9 (2012) 355–371.
[4] B. Ye, J. Jiang, Y. Zhou, J. Liu, K. Wang, Technical and economic analysis of amine-based carbon capture and sequestration at coal-fired power plants, J. Clean. Prod. 222 (2019) 476–487.
[5] D.Y.C. Leung, G. Caramanna, M.M. Maroto-Valer, An overview of current status of carbon dioxide capture and storage technologies, Renew. Sust. Energ. Rev. 39 (2014) 426–443.
[6] P. Feron, A. Cousins, K. Jiang, R. Zhai, S. Shwe Hla, R. Thiruvenkatachari, K. Burnard, Towards zero emissions from fossil fuel power stations, International Journal of Greenhouse Gas Control 87 (2019) 188–202.
[7] Z.H. Liang, W. Rongwong, H. Liu, K. Fu, H. Gao, F. Cao, R. Zhang, T. Sema, A. Henni, K. Sumon, D. Nath, D. Gelowitz, W. Srisang, C. Saiwan, A. Benamor, M. Al-Marri, H. Shi, T. Supap, C. Chan, Q. Zhou, M. Abu-Zahra, M. Wilson,

W. Olson, R. Idem, P. Tontiwachwuthikul, Recent progress and new developments in post-combustion carbon-capture technology with amine based solvents, International Journal of Greenhouse Gas Control 40 (2015) 26–54.
[8] M.N. Anwar, A. Fayyaz, N.F. Sohail, M.F. Khokhar, M. Baqar, W.D. Khan, K. Rasool, M. Rehan, A.S. Nizami, CO_2 capture and storage: a way forward for sustainable environment, J. Environ. Manag. 226 (2018) 131–144.
[9] M. Bui, C.S. Adjiman, A. Bardow, E.J. Anthony, A. Boston, S. Brown, P.S. Fennell, S. Fuss, A. Galindo, L.A. Hackett, J.P. Hallett, H.J. Herzog, G. Jackson, J. Kemper, S. Krevor, G.C. Maitland, M. Matuszewski, I.S. Metcalfe, C. Petit, G. Puxty, J. Reimer, D.M. Reiner, E.S. Rubin, S.A. Scott, N. Shah, B. Smit, J.P.M. Trusler, P. Webley, J. Wilcox, N. Mac Dowell, Carbon capture and storage (CCS): the way forward, Energy Environ. Sci. 11 (2018) 1062–1176.
[10] X. Wang, Q. Guo, J. Zhao, L. Chen, Mixed amine-modified MCM-41 sorbents for CO_2 capture, International Journal of Greenhouse Gas Control 37 (2015) 90–98.
[11] F. Wang, J. Zhao, H. Miao, J. Zhao, H. Zhang, J. Yuan, J. Yan, Current status and challenges of the ammonia escape inhibition technologies in ammonia-based CO_2 capture process, Appl. Energy 230 (2018) 734–749.
[12] K. Han, C.K. Ahn, M.S. Lee, C.H. Rhee, J.Y. Kim, H.D. Chun, Current status and challenges of the ammonia-based CO_2 capture technologies toward commercialization, International Journal of Greenhouse Gas Control 14 (2013) 270–281.
[13] Y. Xu, B. Jin, X. Chen, Y. Zhao, Performance of CO_2 absorption in a spray tower using blended ammonia and piperazine solution: Experimental studies and comparisons, International Journal of Greenhouse Gas Control 82 (2019) 152–161.
[14] F. Shakerian, K. Kim, J.E. Szulejko, J. Park, A comparative review between amines and ammonia as sorptive media for post-combustion CO_2 capture, Appl. Energy 148 (2015) 10–22.
[15] H. Jilvero, F. Normann, K. Andersson, F. Johnsson, Heat requirement for regeneration of aqueous ammonia in post-combustion carbon dioxide capture, International Journal of Greenhouse Gas Control 11 (2012) 181–187.
[16] K. Li, H. Yu, P. Feron, M. Tade, L. Wardhaugh, Technical and energy performance of an advanced, aqueous ammonia-based CO2 capture technology for a 500 MW coal-fired power station, Environmental Science & Technology 49 (2015) 10243–10252.
[17] X. Zhang, R. Zhang, H. Liu, H. Gao, Z. Liang, Evaluating CO_2 desorption performance in CO_2-loaded aqueous tri-solvent blend amines with and without solid acid catalysts, Appl. Energy 218 (2018) 417–429.
[18] M. Zhang, Y. Guo, Rate based modeling of absorption and regeneration for CO_2 capture by aqueous ammonia solution, Appl. Energy 111 (2013) 142–152.
[19] J. Yu, S. Wang, Modeling analysis of energy requirement in aqueous ammonia based CO_2 capture process, International Journal of Greenhouse Gas Control 43 (2015) 33–45.
[20] K. Jiang, K. Li, H. Yu, Z. Chen, L. Wardhaugh, P. Feron, Advancement of ammonia based post-combustion CO_2 capture using the advanced flash stripper process, Appl. Energy 202 (2017) 496–506.
[21] M. Zhang, Y. Guo, Regeneration energy analysis of NH_3-based CO_2 capture process integrated with a flow-by capacitive ion separation device, Energy 125 (2017) 178–185.
[22] B. Decardi-Nelson, A. Akachuku, P. Osei, W. Srisang, F. Pouryousefi, R. Idem, Catalyst performance and experimental validation of a rigorous desorber model for low temperature catalyst-aided desorption of CO_2 in single and blended amine solutions, Journal of Environmental Chemical Engineering 5 (2017) 3865–3872.
[23] H. Shi, A. Naami, R. Idem, P. Tontiwachwuthikul, Catalytic and non catalytic solvent regeneration during absorption-based CO_2 capture with single and blended reactive amine solvents, International Journal of Greenhouse Gas Control 26 (2014) 39–50.
[24] Z. Liang, R. Idem, P. Tontiwachwuthikul, F. Yu, H. Liu, W. Rongwong, Experimental study on the solvent regeneration of a CO_2-loaded MEA solution using single and hybrid solid acid catalysts, AICHE J. 62 (2016) 753–765.
[25] H. Liu, X. Zhang, H. Gao, Z. Liang, R. Idem, P. Tontiwachwuthikul, Investigation of CO_2 regeneration in single and blended amine solvents with and without catalyst, Ind. Eng. Chem. Res. 56 (2017) 7656–7664.
[26] U.H. Bhatti, A.K. Shah, J.N. Kim, J.K. You, S.H. Choi, D.H. Lim, S. Nam, Y.H. Park, I.H. Baek, Effects of transition metal oxide catalysts on MEA solvent regeneration for the post-combustion carbon capture process, ACS Sustain. Chem. Eng. 5 (2017) 5862–5868.
[27] Q. Lai, S. Toan, M.A. Assiri, H. Cheng, A.G. Russell, H. Adidharma, M. Radosz, M. Fan, Catalyst-$TiO(OH)_2$ could drastically reduce the energy consumption of CO_2 capture, Nat. Commun. 9 (2018) 2672–2678.
[28] N. Prasongthum, P. Natewong, P. Reubroycharoen, R. Idem, Solvent regeneration of a CO_2-loaded BEA-AMP Bi-blend amine solvent with the aid of a solid Brønsted Ce $(SO_4)_2/ZrO_2$ superacid catalyst, Energy Fuel 33 (2019) 1334–1343.
[29] G.F. Froment, W.J.H. Dehertog, A.J. Marchi, Zeolite catalysis in the conversion of methanol into olefins, Catalysis 9 (1992) 1–64.
[30] A.S. Al-Dughaither, H.D. Lasa, HZSM-5 Zeolites with different SiO_2/Al_2O_3 ratios. Characterization and NH_3 desorption kinetics, Ind. Eng. Chem. Res. 53 (2014) 15303–15316.
[31] X. Zhang, Y. Huang, H. Gao, X. Luo, Z. Liang, P. Tontiwachwuthikul, Zeolite catalyst-aided tri-solvent blend amine regeneration: an alternative pathway to reduce the energy consumption in amine-based CO_2 capture process, Appl. Energy 240 (2019) 827–841.
[32] X. Zhang, H. Liu, Z. Liang, R. Idem, P. Tontiwachwuthikul, M. Jaber Al-Marri, A. Benamor, Reducing energy consumption of CO_2 desorption in CO_2-loaded aqueous amine solution using Al_2O_3/HZSM-5 bifunctional catalysts, Appl. Energy 229 (2018) 562–576.
[33] M. Magureanu, D. Dobrin, N.B. Mandache, B. Cojocaru, V.I. Parvulescu, Toluene oxidation by non-thermal plasma combined with palladium catalysts, Frontiers in chemistry 1 (2013) 1–6.
[34] V. Loryuenyong, N. Jarunsak, T. Chuangchai, A. Buasri, The photocatalytic reduction of hexavalent chromium by controllable mesoporous anatase TiO_2 nanoparticles, Adv. Mater. Sci. Eng. 2014 (2014) 1–8.
[35] N. Wen, M.H. Brooker, Ammonium carbonate, ammonium bicarbonate, and ammonium carbamate equilibria: a Raman study, J. Phys. Chem. 99 (1995) 359–368.
[36] H. Que, C. Chen, Thermodynamic modeling of the NH_3-CO_2-H_2O system with electrolyte NRTL model, Ind. Eng. Chem. Res. 50 (2011) 11406–11421.
[37] U.H. Bhatti, S. Nam, S. Park, I.H. Baek, Performance and mechanism of metal oxide catalyst-aided amine solvent regeneration, ACS Sustain. Chem. Eng. 6 (2018) 12079–12087.
[38] H. Yang, C. Ma, G. Wang, Y. Sun, J. Cheng, Z. Zhang, X. Zhang, Z. Hao, Fluorine-enhanced Pt/ZSM-5 catalysts for low-temperature oxidation of ethylene, Catalysis Science & Technology 8 (2018) 1988–1996.
[39] U.H. Bhatti, D. Sivanesan, D.H. Lim, S.C. Nam, S. Park, I.H. Baek, Metal oxide catalyst-aided solvent regeneration: a promising method to economize post-combustion CO_2 capture process, J. Taiwan Inst. Chem. Eng. 93 (2018) 150–157.
[40] M. Thommes, K. Kaneko, A.V. Neimark, J.P. Olivier, F. Rodriguez-Reinoso, J. Rouquerol, K.S.W. Sing, Physisorption of gases, with special reference to the evaluation of surface area and pore size distribution (IUPAC Technical Report), Pure Appl. Chem. 87 (2015) 1052–1069.
[41] X. Zhang, Z. Zhu, X. Sun, J. Yang, H. Gao, Y. Huang, X. Luo, Z. Liang, P. Tontiwachwuthikul, Reducing energy penalty of CO_2 capture using Fe promoted SO_4^{2-}/ZrO_2/MCM-41 Catalyst, Environmental Science & Technology 53 (2019) 6094–6102.
[42] X. Zhang, X. Zhang, H. Liu, W. Li, M. Xiao, H. Gao, Z. Liang, Reduction of energy requirement of CO_2 desorption from a rich CO_2-loaded MEA solution by using solid acid catalysts, Appl. Energy 202 (2017) 673–684.
[43] X. Wang, W. Conway, D. Fernandes, G. Lawrance, R. Burns, G. Puxty, M. Maeder, Kinetics of the reversible reaction of CO_2(aq) with ammonia in aqueous solution, J. Phys. Chem. A 115 (2011) 6405–6412.